NANO LETTERS
Letter
Cite This: Nano Lett. 2018, 18, 6222−6228
pubs.acs.org/NanoLett

Programmable Metal/Semiconductor Nanostructures for mRNA-Modulated Molecular Delivery

Libing Zhang,[†,∥] Sae Rin Jean,[‡,∥] Xiyan Li,[§] Tanja Sack,[†] Zongjie Wang,[†] Sharif Ahmed,[†] Gordon Chan,[†] Jagotamoy Das,[†] Alexandre Zaragoza,[†] Edward H. Sargent,[§] and Shana O. Kelley*[,†,‡]

[†]Department of Pharmaceutical Sciences, Leslie Dan Faculty of Pharmacy, University of Toronto, Toronto, Ontario M5S 3M2, Canada

[‡]Department of Chemistry, Faculty of Arts and Science, University of Toronto, Toronto, Ontario M5S 3H6, Canada

[§]Department of Electrical and Computer Engineering, Faculty of Engineering, University of Toronto, Toronto, Ontario M5S 3G4, Canada

Supporting Information

ABSTRACT: Cytotoxic chemotherapeutics are important tools for the clinical treatment of a variety of solid tumors. However, their use is often complicated by multidrug resistance that can develop in patients, limiting the potencies of these agents. New strategies are needed to provide versatile systems that can respond to and disable resistance mechanisms. We demonstrate the use of a new family of materials, programmable metal/semiconductor nanostructures, for drug delivery and mRNA sensing in drug-resistant cells. These materials are composed of a central core gold nanoparticle surrounded by a layer of DNA-capped quantum dots. The modularity of these "core-satellite" assemblies allows for the construction of superstructures with controlled size and the incorporation of multiple functionalities for drug delivery. The DNA sequence within the nanoparticle specifically binds to an mRNA encoding an important drug resistance factor, MRP1, inside cancer cells, releasing a potent anticancer drug doxorubicin. This event triggers a turn-on fluorescence emission along with a downregulation of the MRP1 drug efflux pump, a main resistance factor for doxorubicin, yielding a remarkable improvement in therapeutic efficacy against drug-resistant cancer cells. This work paves the way for the development of programmable materials with multiple synergistic functionalities for biomedical applications.

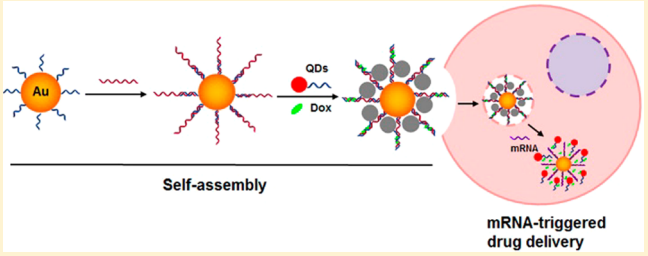

KEYWORDS: *Self-assembly, quantum dots, DNA, multidrug resistance, mRNA*

The emergence of self-assembled nanomaterials has expanded the scope of nanotechnology in biomedical applications including drug delivery, cancer diagnostics, and targeted therapy.[1−4] Nanomaterials have demonstrated excellent tumor-targeting properties due to enhanced permeability and retention in the tumor microenvironment.[5−7] Furthermore, these materials can be rationally designed to deliver therapeutic agents to tumors and to be cleared from the body via the renal system.

Using DNA as a building block for the assembly of nanoparticles allows for programmability within these structure through sequence design.[8−11] DNA also favorably interacts with several anticancer therapeutics such as doxorubicin (Dox) for self-assembly and loading.[12,13] A number of DNA-based systems, including self-assembled DNA 3D nanostructures[14−16] and gold assemblies,[17−19] have been reported for drug delivery. The release of payloads can be triggered by factors like pH,[20] temperature,[21] or other conditions.[22] Ideally, the release of the payloads from designer nanomaterials would be amenable to being monitored and visualized in biological systems.

There remains an unmet need for traceable and biocompatible nanomaterials that can be synthesized in a precisely controllable manner. DNA-capped quantum dots (QDs) have demonstrated excellent optical properties and biocompatibility and have been successfully applied in sensing, targeted tumor imaging, and drug delivery.[23−25] For instance, heterobivalent QD nanoprobes for cancer imaging[26] and photocaged assemblies for catalytic molecular imaging are exciting new classes of tools.[27] DNA-capped QDs can also be easily incorporated into self-assembled systems through DNA hybridization. Recently, programmable self-assembled QD DNA hydrogels with optical tunability have been developed to create versatile nanocarriers for drug delivery.[28] These materials demonstrated high biocompatibility, excellent trackability, and promising therapeutic efficacy.

Chemotherapeutics are an important means of clinical treatment for a variety of cancers. However, their use is often

Received: June 4, 2018
Revised: August 26, 2018
Published: September 6, 2018

DOI: 10.1021/acs.nanolett.8b02263
Nano Lett. 2018, 18, 6222−6228

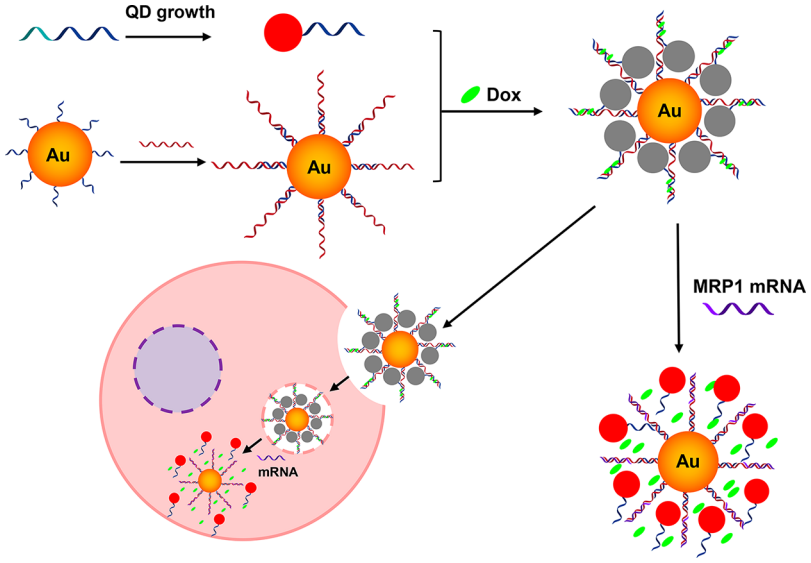

Figure 1. Schematic of the synthesis of self-assembled Au/QD structures loaded with the therapeutic agent Dox, cellular uptake, and drug release. The formation of Au/QD assemblies was achieved through the hybridization of DNA-functionalized Au nanoparticles (NPs) with DNA-capped QDs (photoluminescence quenched) followed by loading with doxorubicin (Dox) for drug delivery. Dox and DNA-capped QDs are released (photoluminescence unquenched) through a strand displacement reaction upon cellular uptake and binding of target MRP1 mRNA.

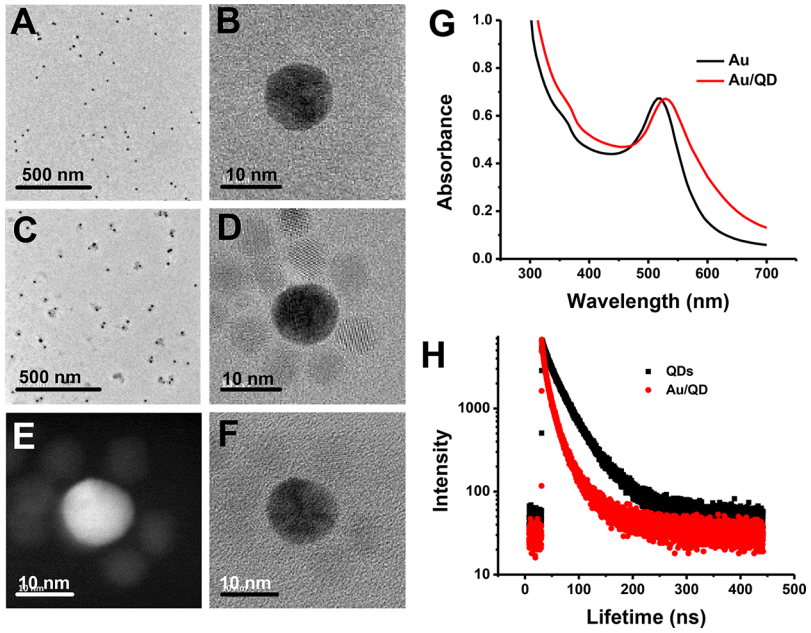

Figure 2. Characterization of Au/QD assemblies. TEM images of (A,B) Au NPs and (C,D) Au/QD assemblies. (E,F) STEM images of Au/QD structures. Scale bars: (A,C) 500 nm and (B,D−F) 10 nm. (G) Absorbance spectra of Au NPs (black line) and Au/QD assemblies (red line) in aqueous solution. (H) Photoluminescence decays of QDs (black line) and Au/QD assemblies (red line) in aqueous solution.

complicated by multidrug resistance (MDR) that can develop in cancer cells. The development of MDR has become an increasingly important problem in cancer therapy[29] as it significantly limits the effectiveness of chemotherapy. One of the most common MDR mechanisms is related to the overexpression of efflux pumps, such as MRP1, that effectively reduce intracellular drug concentrations.[30,31] Some commonly used drugs that are affected by this classical MDR mechanism include: the vinca alkaloids (vinblastine and vincristine), anthracyclines (Dox and daunorubicin), the RNA transcription inhibitor actinomycin-D, and the microtubule-stabilizing drug paclitaxel.[31] The extent of this problem provides a strong rationale for the development of a trackable and intelligent nanomaterial system with controlled drug release that can combat MDR and improve therapeutic efficacy. Whereas strategies to combat drug resistance have been tested in the clinic, including the use of chemical agents targeting efflux pumps or their sources of chemical energy,[32−35] generalizable solutions are still needed.

In this study, we sought to develop a programmable, DNA-based nanomaterial for sensing and controlled release of Dox in cancer cells. The overall goal of the effort was to modulate the activity of efflux pumps directly at the level of gene expression and ultimately enhance the efficacy of this chemotherapeutic. We designed a core−satellite architecture to create DNA-assembled superstructures where a central core

DOI: 10.1021/acs.nanolett.8b02263
Nano Lett. 2018, 18, 6222−6228

gold nanoparticle (Au NP) is encapsulated by a layer of DNA-functionalized QDs (Figure 1). The modularity of this type of DNA-based construct permits the assembly of superstructures with controlled dimensions and multiple functionalities.[3,36] Dox, a potent anticancer drug that preferentially intercalates into DNA duplex GC base pairs, is incorporated into the DNA sequence of the nanomaterial by incubating the materials together.[12] Prior to contact with the target mRNA molecule, the photoluminescence of QDs is quenched by the Au NP due to energy transfer to the metal core. In the presence of target MRP1 mRNA inside cells, DNA-functionalized QDs are released along with Dox during the strand-displacement reaction.[37−39] This strand-displacement reaction provides high specificity in the sensing of a target transcript.[38] This is the first time a Au/QD DNA hybrid nanomaterial has been used for mRNA-triggered drug delivery to combat MDR, and the main features of our unique system include: the ability to (i) inhibit the translation of MRP1 mRNA, (ii) monitor intracellular binding via the recovery of the photoluminescence of DNA-functionalized QDs after release, and (iii) deliver a therapeutic agent into the cancer cells. The combination of these features provides a powerful strategy to combat MDR and enhance therapeutic efficacy.

For the fabrication of core−satellite nanostructures, Au NPs were prepared according to a previously reported method.[40] These nanoparticles have an average diameter of ∼13 nm (Figure 2A,B) and a characteristic absorption at 518 nm (Figure 2G). We used these nanoparticles as a core by grafting them with thiol-modified oligonucleotides. The density of the DNA-modified Au NPs was ∼0.28 DNA per nm^2, which corresponds to a valency of approximately 35−40 DNA strands per particle.

The QDs (quantum yield of 65%) that serve as satellite nanoparticles were synthesized as previously described.[41,42] These particles are CdSe/CdS/ZnS core−shell−shell structures, with the ZnS layer incorporated to provide a higher level of biocompatibility and a lower level of toxicity. The absorbance and emission spectra and TEM image of these QDs were characterized as shown in Figures S1 and S2. The zeta potential measurements for QDs showed that particles had a net negative charge of −24.1 ± 1.6 mV (Figure S3, Supporting Information). The QDs were also grafted with phosphorothioate oligonucleotides, and the formation of DNA-functionalized QDs was confirmed by gel electrophoresis (Figure S4, Supporting Information). Slow-moving DNA functionalized QDs are visualized as a higher band compared with QDs alone.

The metal/semiconductor structures were assembled through DNA hybridization with a complementary linker DNA strand, resulting in the formation of core−satellite nanostructures, as visualized in high-resolution transmission electron microscopy (HRTEM) images (Figure 2C−F). TEM images indicate that a Au NP is surrounded by an average of six to seven QDs. We also investigated the absorption spectra of the Au/QD core−satellite nanostructure and found that the absorption peak had a red shift compared with Au NPs due to the increase in the size of the core−satellite nanostructures (Figure 2G).

After the formation of Au/QD hybrid nanostructures, we investigated in vitro stability in a variety of physiologically relevant environments. First, we evaluated the stability of the structures at biologically relevant pH and in different types of cell media. We observed high stability in the pH range 5.0 to 9.0 (Figure S5, Supporting Information). Next, we incubated the nanostructures in PBS, cell medium, and conditioned cell medium for 24 h at 37 °C to test stability. There was no observable difference in the absorption spectra of the nanoparticle-based structures under these conditions (Figure S6, Supporting Information), indicating that the Au/QD hybrids are stable in cell media. We also studied the enzymatic digestion of these materials. DNase I is a robust enzyme that nonspecifically cleaves single and double-stranded DNA. Incubation of the assemblies with DNase I resulted in a blue shift (Figure S6, Supporting Information), suggesting that DNA sequences in the Au/QD core−satellite nanostructure were degraded. In addition, agarose gel electrophoresis was used to verify the digestion of the Au/QD nanostructure in the presence of different concentrations of DNase I. A distinct band shift was observed with the increase in the concentration of DNase I (Figure S7, Supporting Information), confirming the presence of DNA linkages within the material.

Further characterization of the nanostructures revealed that the photoluminescence of QDs was quenched by Au NPs (Figure S8, Supporting Information). Thus the QDs and Au NPs are close enough in proximity to allow sufficient energy transfer from QDs to Au NPs. The energy transfer was confirmed by measuring the QD donor lifetime using time-correlated single photon counting (TCSPC) (Figure 2H). The photoluminescence lifetime of the QDs was fitted to a biexponential decay in aqueous solution.[43] A short lifetime component of τ_1 = 12.9 ns and a long lifetime component of τ_2 = 37.4 ns and comparable fractional amplitudes were measured (Table 1). Additionally, the photoluminescence lifetime of the QDs was significantly reduced upon interaction with Au NPs (Figure 2H). For the core−satellite nanostructures, biexponential fitting yielded a major short lifetime component of τ_1 = 6.1 ns and a minor long lifetime component of τ_2 = 20.7 ns. The fractional amplitude-weighted mean lifetime of QDs in the absence of Au NPs was τ_{QD} = 28.3 ns, which was considerably reduced when the Au NP acceptor was present in the solution, $\tau_{Au/QD\ NP}$ = 10.6 ns. The energy-transfer efficiency was calculated to be 63% for Au/QD nanostructure using the expression: $(E = 1 - (\tau_{Au/QD\ NP}/\tau_{QD}))$.

Table 1. Photoluminescence Emission Lifetime (ns) (τ) and Fractional Amplitudes (A) of QDs and Au/QD Structures

	$\tau_1/(A_1)$	$\tau_2/(A_2)$
QDs	12.9 (37%)	37.4 (63%)
Au/QD	6.1 (69%)	20.7 (31%)

To validate the ability of Au/QD hybrids to interact with MRP1 mRNA, native polyacrylamide gel electrophoresis (PAGE) was performed (Figure 3A) to monitor complexation. First, we sought to verify the DNA-hybridization driven assembly of the Au/QD nanostructured material. As each DNA sequence was added from lanes 1 to 3, we observed a distinct band shift due to the increase in the weight of the DNA complex. When MRP1 mRNA was added in lane 4, a new band was observed. This result indicates that MRP1 mRNA was successfully hybridized to the linker DNA through a strand displacement reaction. Next, we confirmed target binding by monitoring the change in the photoluminescence of QDs. The noncomplementary DNA strand to MRP1 mRNA was used in the construction of Au/QD nanostructure (control) to test if the target binding was sequence-specific.

DOI: 10.1021/acs.nanolett.8b02263
Nano Lett. 2018, 18, 6222−6228

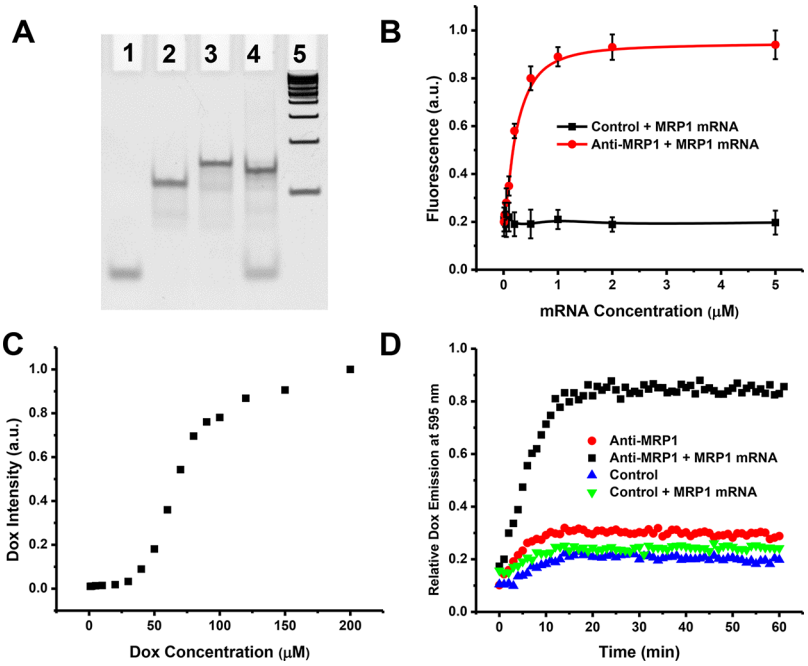

Figure 3. Characterization of the strand displacement reaction in the presence of MRP1 mRNA. (A) Native PAGE analysis to verify self-assembly and strand displacement reaction after the addition of target mRNA. Lane 1: QD-DNA; lane 2: QD-DNA + Linker-DNA; lane 3: QD-DNA + Linker-DNA + Au-DNA; lane 4: QD-DNA + Linker-DNA + Au-DNA + mRNA; lane 5: DNA ladder. (B) Photoluminescence intensity of QDs in control (black line) and anti-MRP1 (red line) Au/QD nanostructures in the presence of MRP1 mRNA. (C) Dox intensity dependence on Dox concentration at fixed DNA concentration. (D) Dox intensity (595 nm) of control and anti-MRP1 Au/QD nanostructures with or without MRP1 mRNA over time.

As shown in Figure 3B, there was no photoluminescence intensity change for the control when MRP1 mRNA was added. In contrast, photoluminescence intensity increased as the MRP1 mRNA concentration was increased when Au/QD nanostructure contained the complementary DNA sequence (anti-MRP1). Therefore, QD release from the core Au NP is highly dependent on the DNA sequence of the competing oligonucleotide. The range of mRNA concentrations tested was selected to match the levels that would be encountered inside of the cell and indicates that the strand displacement reaction designed into these materials is operable at relevant concentrations of triggering mRNA.

To demonstrate the utility of our Au/QD nanostructure for drug delivery, a potent anticancer drug Dox was selected as a model. Dox preferentially intercalates into DNA GC base pairs, permitting facile loading of the drug into the DNA-based material. The innate fluorescence of Dox is stoichiometrically quenched by DNA, and thus drug release can be easily quantified. Figure 3C shows a sequential increase in the Dox fluorescence intensity when a fixed concentration of DNA was incubated with increasing concentrations of Dox. From the titration, the loading capacity of the designed DNA sequences was determined to be eight Dox molecules per DNA duplex. Next, we investigated whether Dox can be released from the Au/QD nanostructure when target mRNA is bound by measuring the fluorescence intensity of Dox. A negligible change in Dox fluorescence was observed in both the presence and absence of MRP1 mRNA when incubated with the control Au/QD assembly (Figure 3D). In contrast, the fluorescence intensity of Dox increased gradually over time when MRP1 mRNA was incubated with anti-MRP1 Au/QD nanostructure with the complementary sequence. Negligible changes were observed in the absence of MRP1 mRNA. Taken together, we can conclude that the system we designed can specifically sense and target MRP1 mRNA with subsequent release of Dox and QDs.

For biomedical applications, it is crucial that these Au/QD hybrids permeate cells and target MRP1 mRNA intracelluarly with high specificity. First, flow cytometry was used to assess the cellular uptake based on the photoluminescence intensity of QDs (Figure 4A). Higher cellular uptake was observed when cells were treated with anti-MRP1 Au/QD assemblies when compared with the control. This result suggests that QDs are only released when cells are treated with anti-MRP1 sequence containing materials and not with the controls. Confocal imaging of treated cells further verified this finding, where high fluorescence was only observed in cells treated with anti-MRP1 Au/QD assemblies (Figure 4B). Quantification of the fluorescence intensity in these microscopy images revealed that there was a 7.5-fold difference between these images (Figure 4C). We directly compared the cellular localization of Dox, QDs, and Dox-QDs using fluorescence microscopy (Figure S9, Supporting Information). In contrast with the extranuclear staining of QDs, we observed a high nuclear localization with DOX-anti-MRP1 similar to Dox, indicating that we were able to successfully release Dox intracellularly. In addition, inductively coupled plasma atomic emission spectroscopy (ICP-AES) was also used to quantify cellular uptake of the Au/QD assemblies through measuring the cadmium concentration. As shown in Figure S10, we can see that the uptake of Au/QD assemblies is much higher than that of free QDs. These findings demonstrate that our programmable Au/QD materials can permeate cells with enhanced cellular uptake and bind specifically to MRP1 mRNA, displacing DNA-functionalized QDs.

DOI: 10.1021/acs.nanolett.8b02263
Nano Lett. 2018, 18, 6222−6228

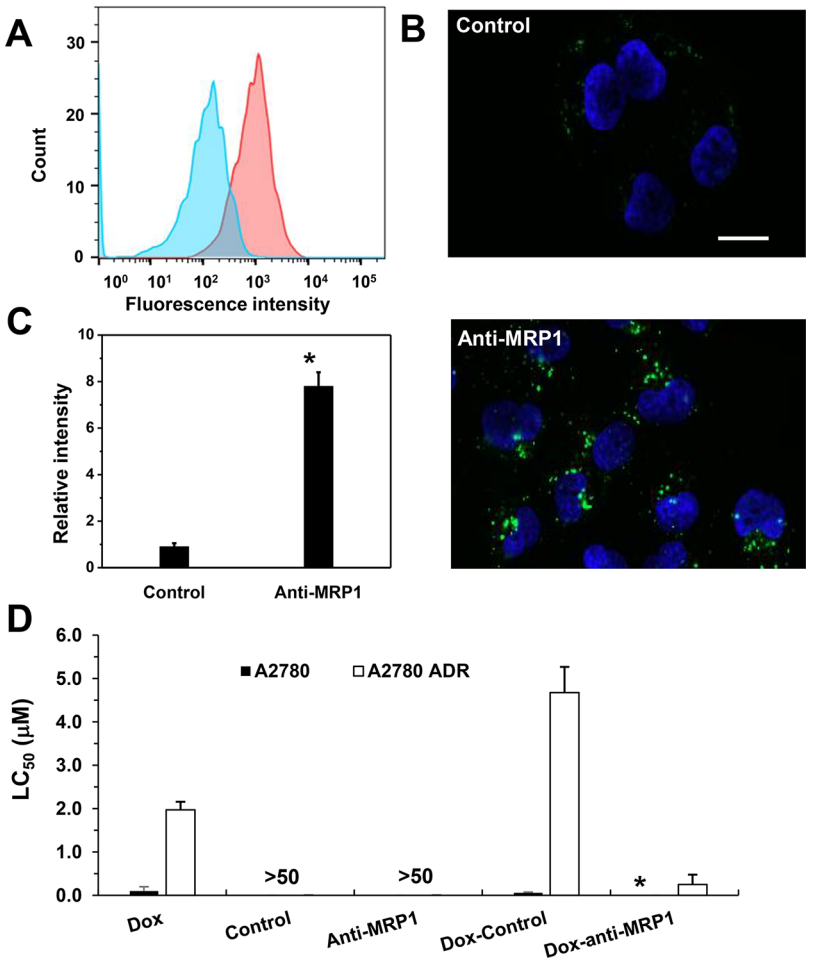

Figure 4. Uptake of Au/QD assemblies in cells, LC_{50}, and gene expression analysis. (A) Flow cytometry analysis of cellular uptake of control (blue) and anti-MRP1 (red) Au/QD assemblies in MDA-MB-231 cells following 7 h of incubation. (B) Confocal microscopy images of control and anti-MRP1 Au/QD assemblies (green) excluded from nuclei (blue) in MDA-MB-231 cells. Scale bars are 10 μm. (C) Fold difference in fluorescence intensity obtained from confocal images of control and anti-MRP1 Au/QD assemblies. *t* test versus control, $p^* < 0.05$. (D) Comparison of LC_{50} values of Dox-anti-MRP1, Dox-control, and free Dox at 72 h in A2780 (Dox-sensitive) and A2780 ADR (Dox-resistant) cells. *Note: value labeled as <0.05.

Finally, we explored the programmable metal/semiconductor hybrids for applications in drug delivery. We compared the LC_{50} values of Dox-anti-MRP1 to the Dox-control and free Dox and found that Dox-anti-MRP1 was 15 times more potent following 72 h of treatment with this panel of agents (Figure S11, Supporting Information). We posited that this may due to the reduction of MRP1 expression and the release of Dox in the vicinity of the site of action, the nuclear genome in this case, which results in higher retention of the drug. This sequence-specific release of Dox can be leveraged to specifically release Dox in cancer cells that typically have a higher expression of MRP1. Gene expression analysis was used to verify silencing of MRP1 because reducing the expression of the corresponding efflux pump should lead to higher retention of Dox. RT-qPCR (real-time quantitative polymerase chain reaction) was used to measure gene expression in cells treated with control and anti-MRP1 Au/QD nanostructures. Interestingly, the quantification of MRP1 transcripts showed that there is a marked decrease in MRP1 expression in anti-MRP1 Au/QD nanostructure-treated cells compared with control (Figure S12 and Table S1, Supporting Information). Flow cytometry was used to probe expression of MRP1 at the protein level. Lower protein expression was observed when cells were treated with anti-MRP1 Au/QD assemblies when compared with the control (Figure S13, Supporting Information), supporting the notion that the Au/QD hybrid materials are able to suppress the expression of a resistance factor.

To further demonstrate that Dox-anti-MRP1 can overcome resistance mechanisms to increase therapeutic efficacy, a pair of human ovarian carcinoma cell lines, A2780 and Dox-resistant cell line A2780 ADR, was used to evaluate the effect of Dox-anti-MRP1 on cell proliferation and viability. As shown in Figure 4D, the LC_{50} values measured indicate that Dox-anti-MRP1 can reduce the viability of both Dox-sensitive and Dox-resistant cell lines. On the basis of the above results, we can conclude that the DNA-directed metal/semiconductor hybrids can indeed overcome MDR to increase the potency of the drug.

The work described here highlights the use of self-assembled DNA-based nanostructures to monitor and mediate drug delivery. We demonstrated that programmable hybrid metal/semiconductor nanostructures can engage with the target MRP1 mRNA, which, in turn, reduces the MRP1 expression and results in a detectable turn-on fluorescence signal and Dox release. Thus the Dox-anti-MRP1 hybrid is significantly more cytotoxic against cancer cells. More importantly, Dox-anti-

DOI: 10.1021/acs.nanolett.8b02263
Nano Lett. 2018, 18, 6222−6228

MRP1 displayed a remarkably improved cytotoxicity in a drug-resistant cell line, validating the potential of this strategy to overcome MDR and effectively enhance the therapeutic efficacy. It is noteworthy, however, that the system reported achieved only ∼50% knockdown of MRP1 expression even after optimization, indicating that this approach cannot achieve quantitative knockdown. Future directions for this work will include incorporating spatiotemporal control of the drug release of biologically active compounds in cellular and animal models. Nonetheless, the current study presents a new strategy for sensing-mediated drug release from DNA-nanoparticle assembled superstructures and further promotes the development of assembled nanomaterials with multiple synergistic functionalities for biomedical applications.

■ ASSOCIATED CONTENT

Supporting Information

The Supporting Information is available free of charge on the ACS Publications website at DOI: 10.1021/acs.nanolett.8b02263.

Materials and methods, DNA and RNA sequences, and additional figures, including absorbance and photoluminescence spectra, TEM and agarose gel images, comparison of LC_{50} values, and RT-qPCR data. (PDF)

■ AUTHOR INFORMATION

Corresponding Author

*E-mail: shana.kelley@utoronto.ca.

ORCID

Jagotamoy Das: 0000-0003-2724-1827
Edward H. Sargent: 0000-0003-0396-6495
Shana O. Kelley: 0000-0003-3360-5359

Author Contributions

‖L.Z. and S.R.J. contributed equally to this work. The manuscript was written with input from all authors. All authors have given approval to the final version of the manuscript.

Notes

The authors declare no competing financial interest.

■ ACKNOWLEDGMENTS

This research is supported by the Canadian Institutes of Health Research (Foundation Grant: FDN-148415) and the Natural Sciences and Engineering Research Council of Canada (Discovery Grant: 2016-06090).

■ REFERENCES

(1) Yan, J.; Hu, C.; Wang, P.; Zhao, B.; Ouyang, X.; Zhou, J.; Liu, R.; He, D.; Fan, C.; Song, S. *Angew. Chem., Int. Ed.* **2015**, *54* (8), 2431−2435.
(2) Angell, C.; Xie, S.; Zhang, L.; Chen, Y. *Small* **2016**, *12* (9), 1117−1132.
(3) Chou, L. Y. T.; Zagorovsky, K.; Chan, W. C. W. *Nat. Nanotechnol.* **2014**, *9* (2), 148−155.
(4) Li, S.; Jiang, Q.; Liu, S.; Zhang, Y.; Tian, Y.; Song, C.; Wang, J.; Zou, Y.; Anderson, G. J.; Han, J.-Y.; Chang, Y.; Liu, Y.; Zhang, C.; Chen, L.; Zhou, G.; Nie, G.; Yan, H.; Ding, B.; Zhao, Y. *Nat. Biotechnol.* **2018**, *36*, 258.
(5) Conde, J.; Doria, G.; Baptista, P. *J. Drug Delivery* **2012**, *2012*, 12.
(6) Conde, J.; Oliva, N.; Artzi, N. *Proc. Natl. Acad. Sci. U. S. A.* **2015**, *112* (11), E1278−E1287.
(7) Yuan, P.; Zhang, H.; Qian, L.; Mao, X.; Du, S.; Yu, C.; Peng, B.; Yao, S. Q. *Angew. Chem., Int. Ed.* **2017**, *56* (41), 12481−12485.
(8) Jones, M. R.; Seeman, N. C.; Mirkin, C. A. *Science* **2015**, *347* (6224), 1260901.
(9) Surana, S.; Shenoy, A. R.; Krishnan, Y. *Nat. Nanotechnol.* **2015**, *10* (9), 741−747.
(10) Edwardson, T. G. W.; Lau, K. L.; Bousmail, D.; Serpell, C. J.; Sleiman, H. F. *Nat. Chem.* **2016**, *8* (2), 162−170.
(11) Li, Y.; Liu, Z.; Yu, G.; Jiang, W.; Mao, C. *J. Am. Chem. Soc.* **2015**, *137* (13), 4320−4323.
(12) Xiao, Z.; Ji, C.; Shi, J.; Pridgen, E. M.; Frieder, J.; Wu, J.; Farokhzad, O. C. *Angew. Chem., Int. Ed.* **2012**, *51* (47), 11853−11857.
(13) Qiu, L.; Chen, T.; Öçsoy, I.; Yasun, E.; Wu, C.; Zhu, G.; You, M.; Han, D.; Jiang, J.; Yu, R.; Tan, W. *Nano Lett.* **2015**, *15* (1), 457−463.
(14) Chang, M.; Yang, C.-S.; Huang, D.-M. *ACS Nano* **2011**, *5* (8), 6156−6163.
(15) Zhang, Q.; Jiang, Q.; Li, N.; Dai, L.; Liu, Q.; Song, L.; Wang, J.; Li, Y.; Tian, J.; Ding, B.; Du, Y. *ACS Nano* **2014**, *8* (7), 6633−6643.
(16) Lee, H.; Lytton-Jean, A. K. R.; Chen, Y.; Love, K. T.; Park, A. I.; Karagiannis, E. D.; Sehgal, A.; Querbes, W.; Zurenko, C. S.; Jayaraman, M.; Peng, C. G.; Charisse, K.; Borodovsky, A.; Manoharan, M.; Donahoe, J. S.; Truelove, J.; Nahrendorf, M.; Langer, R.; Anderson, D. G. *Nat. Nanotechnol.* **2012**, *7*, 389.
(17) Alexander, C. M.; Hamner, K. L.; Maye, M. M.; Dabrowiak, J. C. *Bioconjugate Chem.* **2014**, *25* (7), 1261−1271.
(18) Gossai, N. P.; Naumann, J. A.; Li, N.-S.; Zamora, E. A.; Gordon, D. J.; Piccirilli, J. A.; Gordon, P. M. *Oncotarget* **2016**, *7* (25), 38243−38256.
(19) Raeesi, V.; Chou, L. Y. T.; Chan, W. C. W. *Adv. Mater.* **2016**, *28* (38), 8511−8518.
(20) Sun, W.; Jiang, T.; Lu, Y.; Reiff, M.; Mo, R.; Gu, Z. *J. Am. Chem. Soc.* **2014**, *136* (42), 14722−14725.
(21) Yang, X.; Liu, X.; Liu, Z.; Pu, F.; Ren, J.; Qu, X. *Adv. Mater.* **2012**, *24* (21), 2890−2895.
(22) Mo, R.; Jiang, T.; Sun, W.; Gu, Z. *Biomaterials* **2015**, *50*, 67−74.
(23) Ma, N.; Sargent, E. H.; Kelley, S. O. *Nat. Nanotechnol.* **2009**, *4* (2), 121−125.
(24) Wang, G.; Li, Z.; Ma, N. *ACS Chem. Biol.* **2018**, *13*, 1705−1713.
(25) Ma, N.; Tikhomirov, G.; Kelley, S. O. *Acc. Chem. Res.* **2010**, *43* (2), 173−180.
(26) Wei, W.; He, X.; Ma, N. *Angew. Chem., Int. Ed.* **2014**, *53* (22), 5573−5577.
(27) Shen, Y.; Li, Z.; Wang, G.; Ma, N. *ACS Sens* **2018**, *3* (2), 494−503.
(28) Zhang, L.; Jean, S. R.; Ahmed, S.; Aldridge, P. M.; Li, X.; Fan, F.; Sargent, E. H.; Kelley, S. O. *Nat. Commun.* **2017**, *8* (1), 381.
(29) Gottesman, M. M.; Fojo, T.; Bates, S. E. *Nat. Rev. Cancer* **2002**, *2* (1), 48−58.
(30) Higgins, C. F. *Nature* **2007**, *446* (7137), 749−757.
(31) Cole, S. P. *Annu. Rev. Pharmacol. Toxicol.* **2014**, *54*, 95−117.
(32) Ye, M.; Han, Y.; Tang, J.; Piao, Y.; Liu, X.; Zhou, Z.; Gao, J.; Rao, J.; Shen, Y. *Adv. Mater.* **2017**, *29* (38), 1702342.
(33) Tian, Y.; Jiang, X.; Chen, X.; Shao, Z.; Yang, W. *Adv. Mater.* **2014**, *26* (43), 7393−7398.
(34) Wang, F.; Wang, Y.-C.; Dou, S.; Xiong, M.-H.; Sun, T.-M.; Wang, J. *ACS Nano* **2011**, *5* (5), 3679−3692.
(35) Cho, M. H.; Kim, S.; Lee, J.-H.; Shin, T.-H.; Yoo, D.; Cheon, J. *Nano Lett.* **2016**, *16* (12), 7455−7460.
(36) He, X.; Zeng, T.; Li, Z.; Wang, G.; Ma, N. *Angew. Chem., Int. Ed.* **2016**, *55* (9), 3073−3076.
(37) Zhang, D. Y.; Winfree, E. *J. Am. Chem. Soc.* **2009**, *131* (47), 17303−17314.
(38) Zhang, L.; Zhu, J.; Zhou, Z.; Guo, S.; Li, J.; Dong, S.; Wang, E. *Chem. Sci.* **2013**, *4* (10), 4004−4010.
(39) Du, Y.; Pothukuchy, A.; Gollihar, J. D.; Nourani, A.; Li, B.; Ellington, A. D. *Angew. Chem., Int. Ed.* **2017**, *56* (4), 992−996.
(40) Grabar, K. C.; Freeman, R. G.; Hommer, M. B.; Natan, M. *Anal. Chem.* **1995**, *67* (4), 735−743.

DOI: 10.1021/acs.nanolett.8b02263
Nano Lett. 2018, 18, 6222−6228

(41) Yu, W. W.; Qu, L.; Guo, W.; Peng, X. *Chem. Mater.* **2003**, *15* (14), 2854−2860.
(42) Chen, O.; Zhao, J.; Chauhan, V. P.; Cui, J.; Wong, C.; Harris, D. K.; Wei, H.; Han, H.-S.; Fukumura, D.; Jain, R. K.; Bawendi, M. G. *Nat. Mater.* **2013**, *12* (5), 445−451.
(43) Yaghini, E.; Giuntini, F.; Eggleston, I. M.; Suhling, K.; Seifalian, A. M.; MacRobert, A. J. *Small* **2014**, *10* (4), 782−792.

DOI: 10.1021/acs.nanolett.8b02263
Nano Lett. 2018, 18, 6222−6228